Available online at www.sciencedirect.com

jmr&t Journal of Materials Research and Technology

www.jmrt.com.br

Original Article

Microstructural variations at different distance from the surface in forged 18 Ni C300 maraging steel

Nathália Cândido Figueiredo[a,*], *Carlos Augusto Silva de Oliveira*[a], *Mohammad Masoumi*[b], *Hamilton Ferreira Gomes de Abreu*[c]

[a] *Department of Mechanical Engineering, Forming Laboratory of Materials, Federal University of Santa Catarina, Florianópolis, SC, Brazil*
[b] *Department of Metallurgical and Materials Engineering, Phase Transformation Laboratory, University of São Paulo, São Paulo, SP, Brazil*
[c] *Department of Metallurgical and Materials Engineering, Characterization Laboratory of Materials, Federal University of Ceará, Fortaleza, CE, Brazil*

ARTICLE INFO

Article history:
Received 18 July 2017
Accepted 19 January 2018
Available online 16 March 2018

Keywords:
Strain distribution
Maraging steel
EBSD
Grain orientation

ABSTRACT

Microstructure and microtexture of forged 18 Ni C300 maraging steel at different solution annealed temperatures were studied to show strain distribution associated with forged surface distance. Samples were examined by Electron Back-Scattered Diffraction to characterize the microstructural parameters such as grain sizes, grain orientation and boundary characteristics throughout the forged samples at the surface, quarter depth and centre areas. The results showed a grain refinement across the forging depth, without changing its hardness. In addition, the textural variation was highly dependent on the value of local strain during forging processing. A high number of grains oriented along {001} planes parallel to forging direction (FD) were formed close to the forged surface. While, {110}//FD and {111}//FD texture fibres developed significantly by increasing the distance of forged surface.

1. Introduction

Maraging steels exhibit a fully martensitic structure at solution treatment at any cooling rate because of a high amount of nickel content and absence of carbon in body-centre cubic structure. These are mainly used in aerospace, military and production tooling where excellent combination of mechanical properties, toughness and good corrosion resistance are required [1–3].

Forging is one of the common fabrication and forming technique in high strength steels including Maraging 18 Ni steels. The forging process is characterized by the formation of heterogeneous microstructures along the forged surface contact. For example, dead-metal zone at the top and bottom and slip-lines generate by forging because of the friction at the

* *Corresponding author.*
E-mail: nathaliacfigueiredo@gmail.com (N.C. Figueiredo).

https://doi.org/10.1016/j.jmrt.2018.01.007

interface between the specimen and the forge dies. The friction prevents radial expansion in contact with the die [4,5]. These are resulted of non-uniform distribution of stresses and strains during the process at different distance of forged surface. Furthermore, forging process in Maraging 18 Ni steels produces refinement of the martensite microstructure, particularly when the phase transformation from austenite to martensite occurs from a work-hardened austenite. An acceleration of the precipitation and reverted austenite formation kinetics are induced in the ausformed martensite also happens during the forging process of Maraging steels [6]. It is well known that the microstructure changes such as prior austenite grain size and precipitations influence the mechanical properties of maraging steels [2,7,8]. Hou et al. [9] studied the effect of solution-annealing treatment on reverted austenite, prior austenite grain size, and its effects on final mechanical and fracture absorbing energy behaviour. They showed that the extreme grain growth occurred during solution-annealing above 950 °C, and dropped the mechanical and toughness properties. In addition, the Ni_3(Ti,Mo) precipitates have a significant influence on the strength and toughness [10]. Li et al. [10] reported that Ni_3(Ti,Mo) precipitate and reverted austenite are the critical factors influencing the strength and toughness. The Ni_3(Ti, Mo) precipitate in the weld metal improves the strength of welded joints as its volume fraction increases. The reverted austenite in grain boundaries is harmful to the toughness of welded joints, while the reverted austenite in the matrix is beneficial to the toughness of welded joints because of its finely dispersive distribution and its ability to prevent crack propagation. Increasing the amount of reverted austenite in the matrix is an effective way to improve mechanical properties [10].

The effect of microstructural, crystallographic orientations and grain boundary distributions on mechanical properties is well studied [11–13]. In addition, the levels of induced deformation across the forging direction of samples can have a remarkable effect on developing shear bands and final properties. The aim of the current study was to understanding the effect of strain distribution on microstructure and microtexture evolutions at different distance from forged surface.

2. Material and experimental procedures

The material used in the present study was taken from a 20 mm thick disc with 170 mm diameter. The chemical composition of the alloy 18Ni C300 maraging steel is listed in Table 1, given by CTM-SP. Prismatic samples were cut out from the disc and then machined to the dimensions 10 × 55 × 15 mm. Then, the samples were solution annealed at 950 and 1100 °C temperatures for 1 h followed by water quenching. Solution treatment was performed at two different temperatures to estimate the effect of prior austenite grain size in the forging process. In order to prevent the formation of Ni_3(Ti,Mo) precipitates that would facilitate crack formation during hot deformation, forging was conducted at 350 °C. So the solution treated samples were heated at 350 °C for 30 min and then warm forged between flat dies surfaces by uniaxial compression without lubrication, in a 150 Ton friction drive screw, to achieve a height reduction of 30%. Immediately the samples were water quenched after forging processing.

Table 1 – Chemical composition of 18Ni C300 maraging steel.

	Ni	Co	Mo	Ti	C	S	Fe
% wt	18.41	9.35	5.04	0.78	0.008	0.0011	Balance

To estimate the effect of strain distribution on forged conditions, microstructural parameters such as microstructure and hardness were analyzed at different distance from forged surface. Additionally, Electron Back-Scattered Diffraction (EBSD) was utilized to aid in better understanding the evaluation of crystallographic orientation changes along forging direction.

Both forged samples were sectioned along central plane perpendicular to the forging axis. The sectioned samples were mounted in Bakelite and prepared following standard grinding up to 1200 grit paper, then polished with 3 and 1 μm diamond paste and final 0.04 μm colloidal silica polishing for a period of 90 min. EBSD examination was carried out on a FEI XL30 Scanning Electron Microscope (SEM) equipped with Oxford Instruments HKL Channel 5 data acquisition and analysis software. An operating voltage of 25 kV was used to optimize the diffraction patterns of BCC martensite Kikuchi pattern. Three EBSD scans of the forged material at the surface, quarter depth and centre were performed. For each EBSD examination an indexing rate of at least 65% was achieved. The EBSD data was analyzed for grain size, boundary characteristics and crystallographic texture using MTEX – free and open source software toolbox and Channel 5 data acquisition. The Vickers hardness (HV) testing was conducted at a load of 1 kgf and a holding time of 15 s, according to ASTM E384 standard, using a SHIMADZU HMV2 Vickers hardness instrument. The measurements were carried out on the same regions of the EBSD maps.

3. Results

Shear band with crack were formed at surface contact and grown approximately 45° inclined to the contact-forged surface through the several grains in both samples subjected to different annealing temperatures followed by forging at 350 °C. Figs. 1 and 2 show the microstructure changes as a function of surface distance in both specimens. Additionally, it can be seen a presence of a crack in the shear band for both conditions.

In order to obtain a comprehensive understanding of the microstructural evolution and grain orientation changes across forging direction, EBSD examinations were conducted on the three regions (indicated at A, B an C in Figs. 1 and 2) throughout the forged samples at different distance from forged surface. Normal direction orientation image maps (OIM) parallel to the forging direction (FD) for three different regions of both sample (i.e., surface (A), quarter depth (B), and centre (C)) are presented in Fig. 3.

The variation of average grains sizes and microhardness as a function of surface distance of both forged samples is shown in Fig. 4. Coarser grains were observed in A1100F350 sample due to the growth of austenite grains at higher

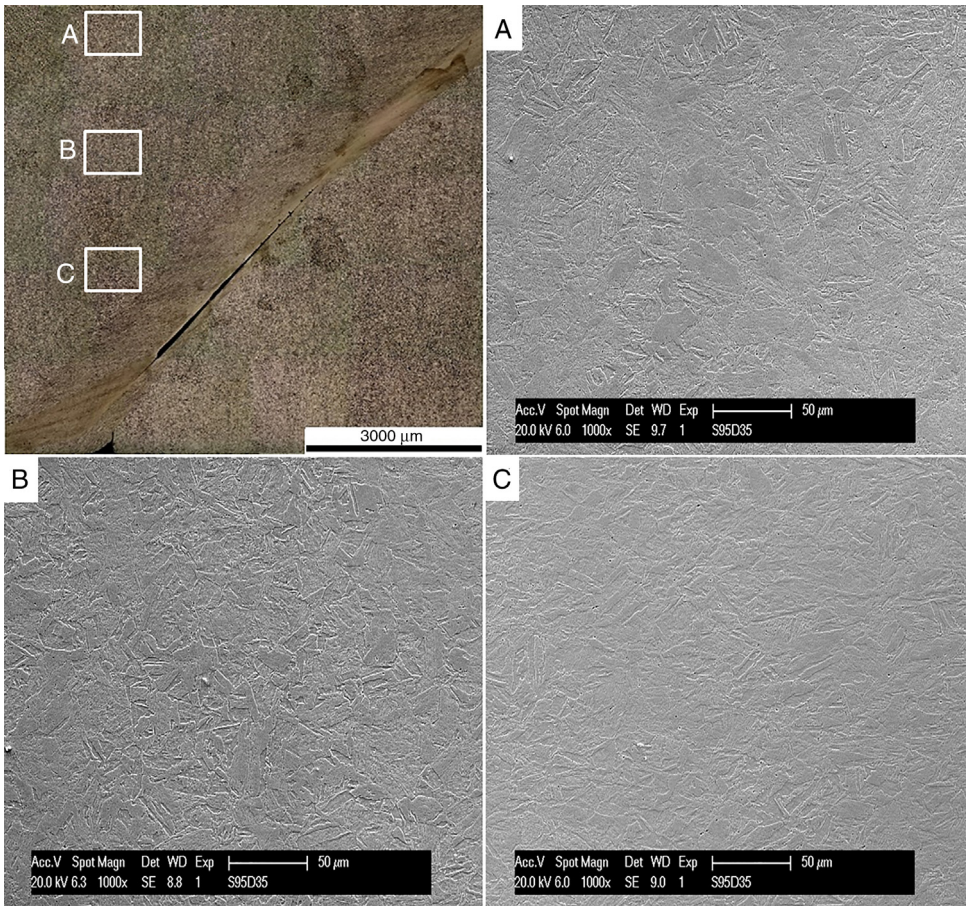

Fig. 1 – Optical and scanning electron images of A950F350 sample as a function of surface distance.

annealing temperature which is consistent with Hou et al. [9] and Lima Filho [14] results. Regions close the surface showed the lowest hardness and gradually increased with surface depth. A fine grain size was formed in A950F350 (about 17%) rather than A1100F350 sample (about 40%).

Fig. 5 presents the variation of boundary distributions of both specimens as a function of surface depths. A tendency of a gradual increase in HABs from surface to centre region and a decrease in the low angle boundaries (LABs) were observed in both forged samples with different annealing temperatures due to grain refinement by strain-induced grain via warm forging.

Furthermore, Kernel average misorientation (KAM) analyzing to estimate the induced-strain distribution during warm forging was analyzed by EBSD data to characterize dislocation tangles in within the individual grains [15], Fig. 6. A gradual decrease in low Kernel frequency and increases in high KAM frequency of A950F350 are in agreement with increasing with increasing the number of grain boundaries due to grain refinement. However, a slight decreasing followed by intense increasing in high KAM values was calculated in A1100F350 sample. This behaviour can be explained by formation of new random grains from sub-grains due to absorbing the dislocation. Thus, increasing the misorientation angle inside the grain led to grain fragment and formation of new grains [16,17].

Accurate retained austenite grains orientation of all investigated samples were calculated and presented by ODF at constant $\varphi_2 = 45^\circ$ in Fig. 7. The crystallographic texture oriented (001)[01$\bar{0}$] was identified in A950F350 sample, and, (001)[23$\bar{0}$] and (1$\bar{1}\bar{3}$)[$\bar{1}$2$\bar{1}$] with approximately 5° deviation from ideal {001} fibre were characterized in A110F350 sample. In general, the {001} grains parallel to forging direction (FD) were characterized in region A, closed the contact surface. However, the formation of (111)[1$\bar{0}$1] corresponding the dense BCC plane and direction can facilitate dislocation slip. The ODF calculation revealed the presence of (11$\bar{1}$)[32$\bar{1}$] and (110)[11$\bar{1}$] orientation at region B of sample A950F350 and A1100F350, respectively. However, a wide distribution of grain orientations can be distinguished in A950F350 sample. As it is expected the similar crystal orientation was developed in region C which suffered more deformation. (111)[11$\bar{0}$] orientation was predominant of both samples as a main slip system in BCC materials due to warm forging. Moreover, (221)[13$\bar{4}$] and (112)[13$\bar{2}$] were intensified in A1100F350 sample.

4. Discussion

Warm forging at 350 °C with reduction to 30% led to the formation of shear bands that passed through several grains in both solution treatment conditions. The friction at the

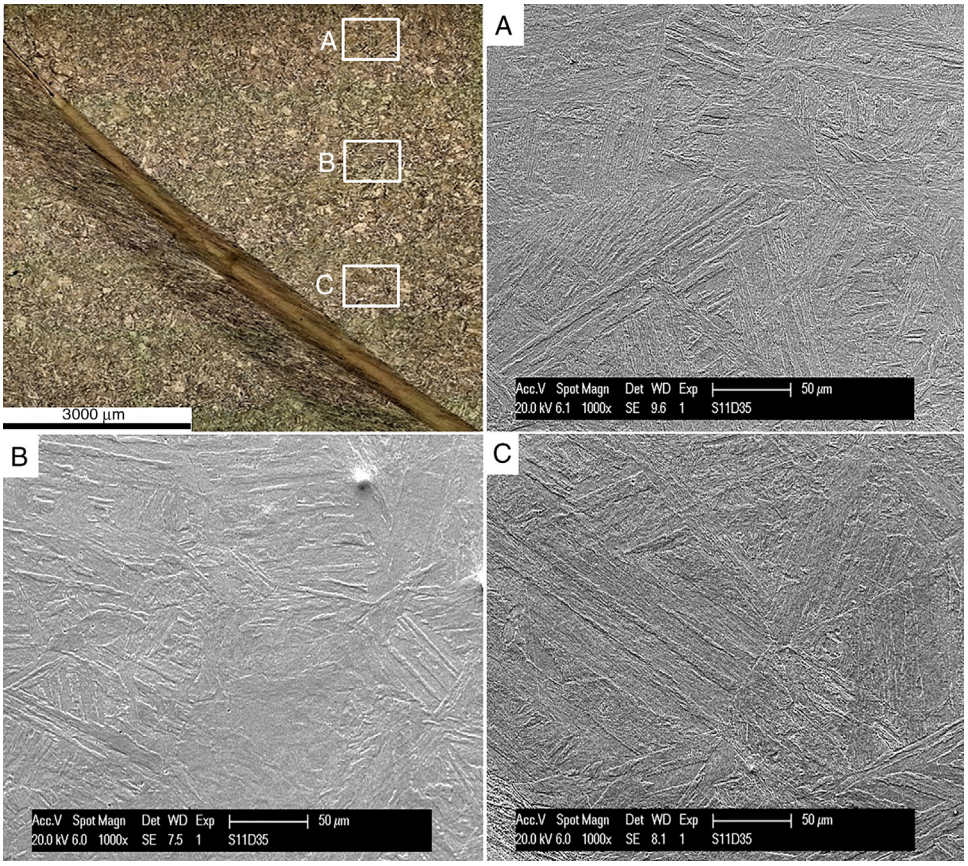

Fig. 2 – Optical and scanning electron images of A1100F350 sample as a function of distance surface.

interface between the specimen and the die prevents radial expansion of material in contact with the die. Consequently, a dead zone was developed because of this restriction. A considerable variation in effective strain across forging direction was induced during forging operation. No correlation was found between shear band and crack propagation with precipitates.

The orientation image maps allowed estimating the strain distribution as well as the level of friction during forging processing. This technique allows estimating the strain distribution using diverse methods such as Kernel average misorientation (KAM) and variation of distortion lattice via point to point misorientation.

Grain size is one of the outstanding microstructural characteristics to determined mechanical properties associated with Hall–Petch [18,19] relationship where strength is inversely dependent on the square root of grain size. Linear intercept technique from optical or scanning electron microscope (SEM) images widely used, which have influenced the manual measurements and subjective interpretation of grain boundary positions associated with the change of contrast due to the etching [20]. EBSD method is an alternative technique that can easily evaluated the grain sizes based on crystallographic orientations of neighbouring crystal and determined the grain boundaries when point-to-point misorientation angle is greater than 15° (and phase boundaries by variation of Kikuchi diffracted pattern) [21]. Presence of the coarser grains at the regions close to the forging surface is associated with low effective strain due to friction effect. Thereby, grain refinement was sluggish at these regions in comparison with the centre zone (area C) with higher levels of deformation. In addition, an inverse relationship was presented between microhardness and average grain size in both specimens which is in agreement with Hall–Petch theory.

Grain boundary characteristics determined by crystallographic orientation and interfaces of neighbouring grains are an effective method to predict mechanical behaviour to prevent grain boundary degradations (i.e., grain boundary sliding [12], segregation-induced embrittlement [13]). It is reported that high angle boundaries with great misorientation angles at neighbouring crystals have higher internal energy, which considered as preferred path for crack propagation [14,15]. However, coincidence site lattice (CSL) boundaries as HABs with special number of coinciding lattice points have low energy orientation dependence grain boundary have higher intergranular crack resistance than high angle boundaries [16,17]. The increase in the HABs can be associated with the higher strain accumulation in centre regions than close to surface areas due to formation the dead zone. In addition, Semiatin et al. [22] reported that the continuous dislocation absorption in subgrain boundaries occurs during material undergoes deformation, resulting in the grain refinement and formation of new set of grains with increasing the number of HABs. Although good lattice consistency of CSL boundaries can control mechanical behaviour, no significant variation was characterized using EBSD data.

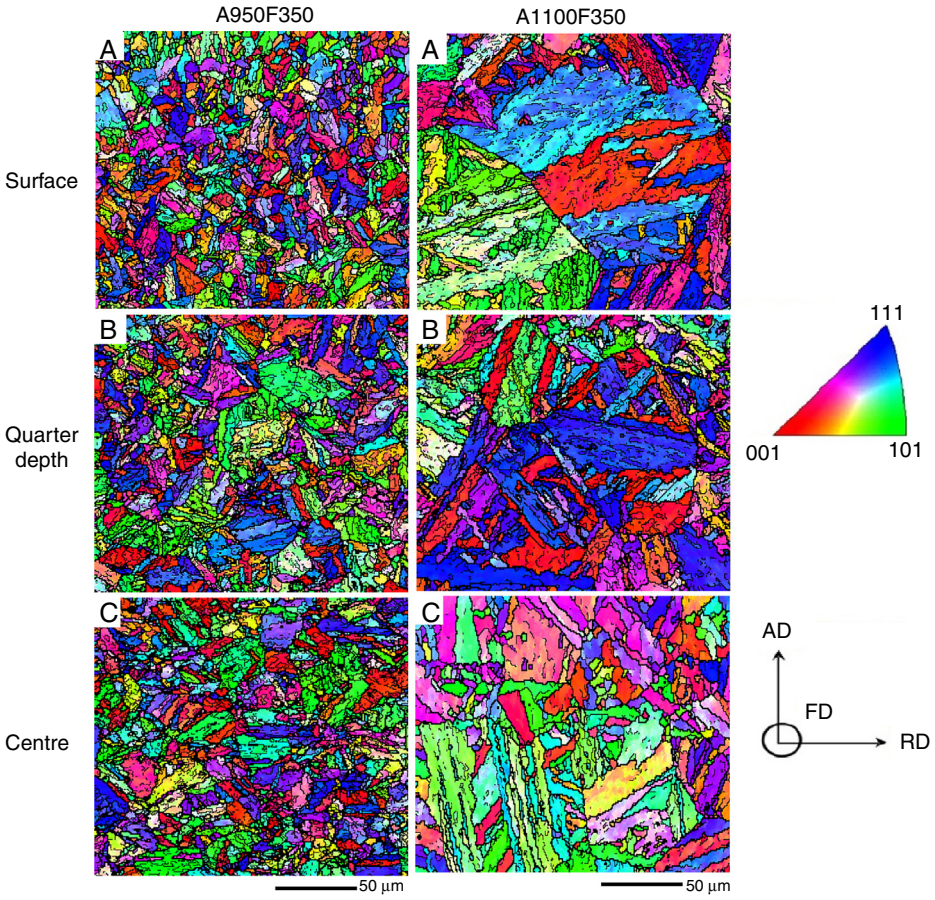

Fig. 3 – OIMs of A950F350 and A1100F350 samples at three different areas referred to Figs. 1 and 2.

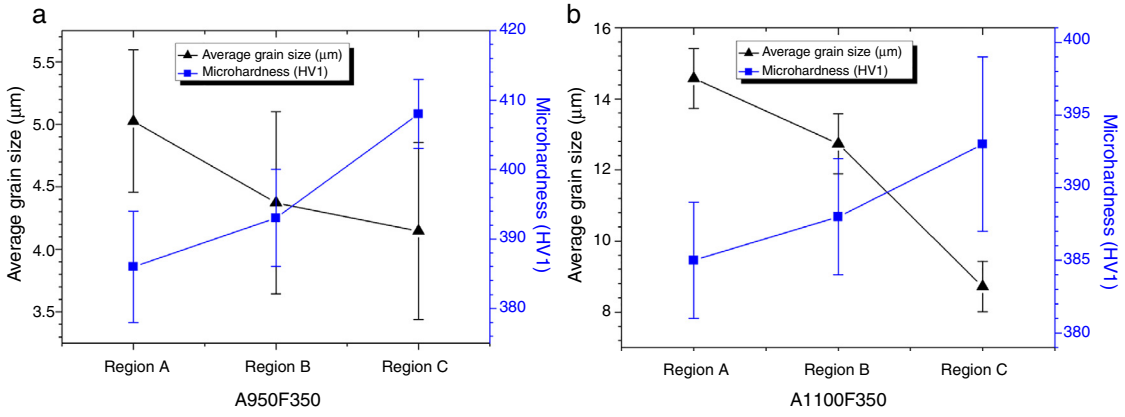

Fig. 4 – Variation of average grains sizes and microhardness as a function of surface distance of (a) A950F350 and (b) A1100F350 forged samples.

The KAM of each point is calculated as the average misorientation angle between each pixel and its specified number (first neighbouring pixels, in this paper) of nearest neighbour or pixels in 2D EBSD data. Moreover, a threshold value for misorientations of maximum 5° was applied to remove the contributions of grain boundaries and intra-granular strain caused by interstitial supersaturation [18,23]. In general, KAM analyzing can provide better extermination of localized strain distribution due to dislocation cell and sub-grains associated the reference orientation deviation. Low KAM values (KAM < 1°) indicate the presence of low internal grains with low internal energy due to very low number of dislocations within the grain. However, high Kernel amounts (KAM > 3°) are mainly considered the strain accumulation, dislocation walls, and dislocation structures near grain boundaries. Moreover, this strain amplitude promotes expansion of the wall-cell

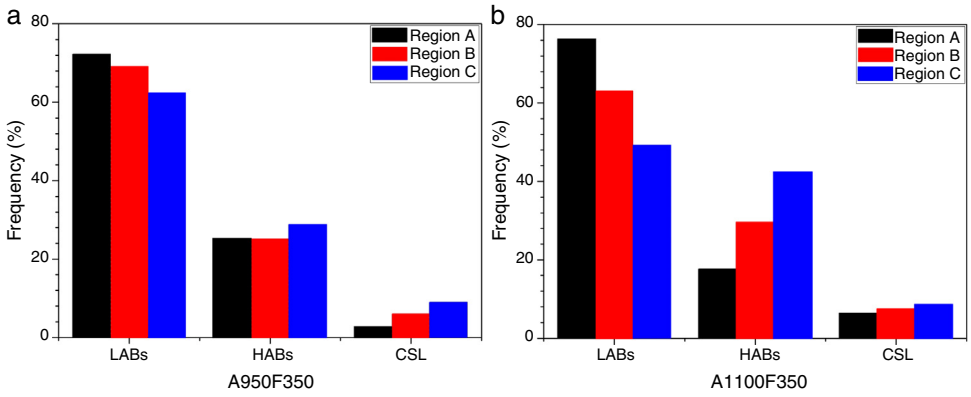

Fig. 5 – Variation of grain boundary distribution as a function of surface distance of (a) A950F350 and (b) A1100F350 forged samples (LABs: low angle boundaries, HABs: high angle boundaries, and CSL: coincidence site lattice boundaries).

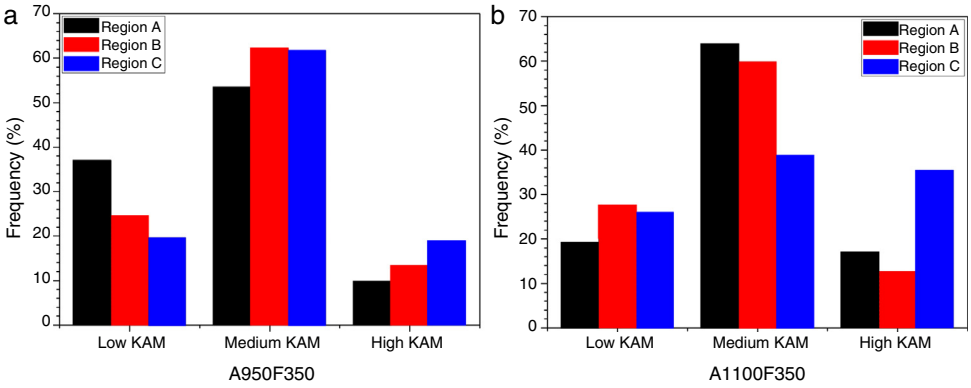

Fig. 6 – Variation of Kernel average misorientatio (KAM) value changes in three different regions of (a) A950F350 and (b) A1100F350 forged samples.

dislocation structure towards the grain interior [19]. In addition, high KAM values reveal the presence of abundant LABs accompanied by the significantly lattice distortion, representing higher dislocation densities and internal energy. Thus, remarkable deviation of lattice orientation by rotations due to the interface lattice misfit is expected.

Cristal Orientation controls the mechanism of plastic deformation by crystallographic dislocation slip. Sainath et al. [24] and Blondé et al. [25] reported the gradual increasing in yield response by means of the orientation dependence from the interatomic forces, i.e., $YS_{\langle 100\rangle} < YS_{\langle 102\rangle} < YS_{\langle 110\rangle} < YS_{\langle 112\rangle} < YS_{\langle 111\rangle}$. The orientation distribution function (ODF) is a mathematical function underlying statistical method using Kernel density estimation describes the frequency of occurrence of particular crystal orientations in a three dimensional Euler space [26]. A conventional description of an orientation in the form $\{hkl\}\langle uvw\rangle$, which $\{hkl\}$ indicates a specific plane parallel to the forging plane and $\langle uvw\rangle$ presents the direction parallel to the forging direction. It is notable that, sample annealed at 1100 °C had recognizable crystallographic texture due to larger grain sizes. The presence of $(221)[13\bar{4}]$ and $(112)[13\bar{2}]$ orientations in A1100F350 sample could be associated with nucleation of new grains due to transformation of low angle or subgrain boundaries into high (random) boundaries, which was explained in boundary and KAM distributions. It is worth mentioning that the {112} planes as dense atomic planes in BCC structure can facilitate dislocation loop and dislocation multiplication [27,28]. In addition, Raabe explained [29] that the adequate slip systems, which were activated by external strain state, reduced due to their geometrical orientation dependence applied force. While, the abundant dislocation densities enhanced crystallographic defects to occurrence of mesoscopic inhomogeneities such as micro- and shear bands. It could be concluded that the orientation changes from {001}//FD components at region close to the sample surface into {110}//FD and {111}//FD particularly at the centre of the forging, indicated a dominant shear deformation texture accompanied with more intense induced-strain.

5. Conclusions

A complete characterization of the microstructural parameters throughout the forged samples with different solution-annealed temperatures was carried out. The following conclusions are made base on the analysis:

- The results clearly show that the strain distribution during forging greatly effects on the microstructure and texture evolution through the materials.

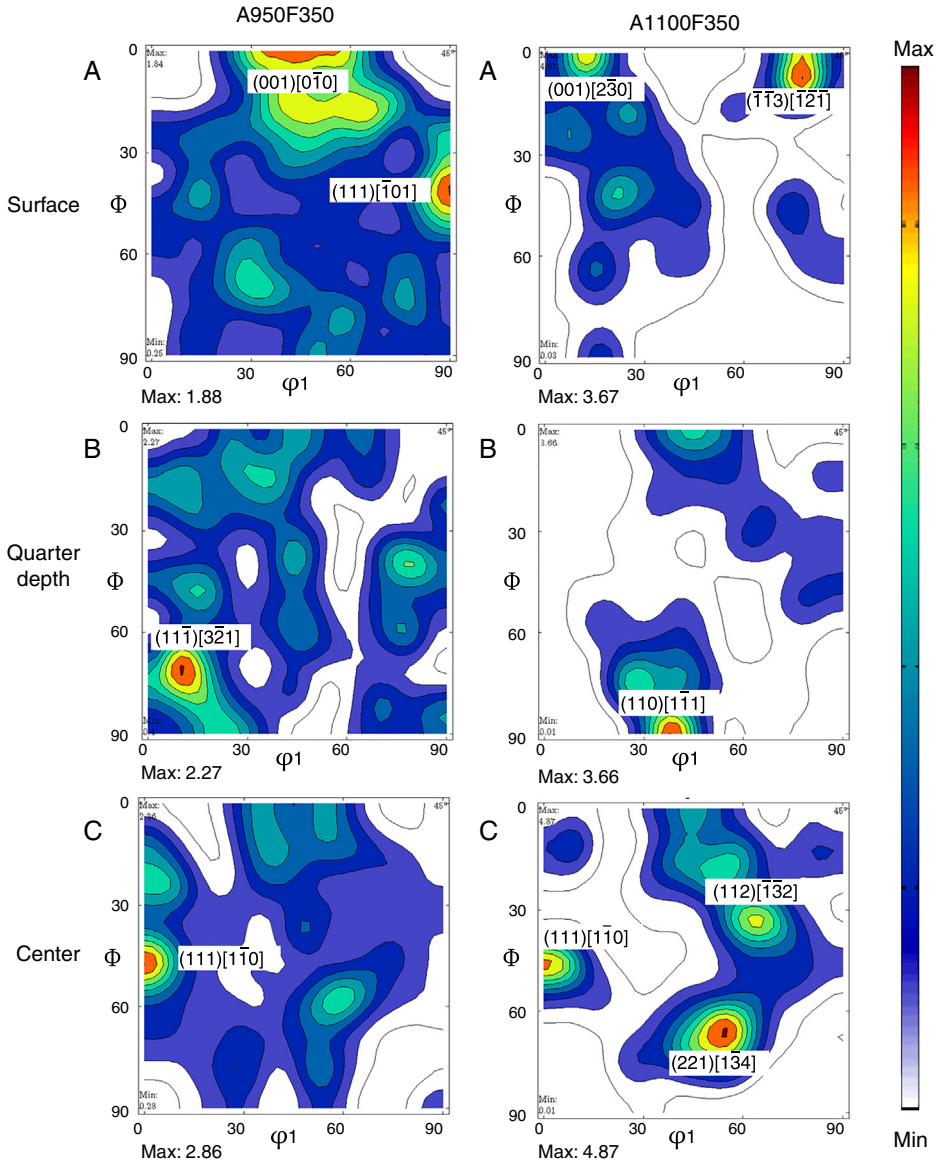

Fig. 7 – ODF of BCC martensitic phase at constant $\varphi_2 = 45°$ of both forged sample at three different regions referred to Figs. 1 and 2.

- No correlation between the formation of shear or deformation bands during warm forging with localized deformation and compositional inhomogeneity were found.
- Close to the surface where strain is a minimum, grain refinement was sluggish in comparison with the centre of the forging blank with higher levels of deformation.
- An increase in hardness is shown on the three regions towards to the centre for both solution temperatures. This behaviour was not significant in the condition of the lowest solution temperature. However, only the centre regions have a true difference between the conditions.
- The results showed that the temperature of solution treatment in maraging steels does not have a significant effect in hardness, besides of promoting a grain growth.
- The warm forging at 350 °C could not avoid formation high dislocation density bands and dislocation accumulation by recovery.
- The {110}//FD and {111}//FD fibres increased with depth, whilst {001} decreases.
- The lowest levels of strain are seen close to the surface with the least dislocation tangles amount, then gradually increasing to reach a maximum at the forging centre where a number of dislocation tangles are greatest.

Conflicts of interest

The authors declare no conflicts of interest.

Acknowledgments

The authors would like to acknowledge the support grant given by Coordenação de Aperfeiçoamento de Pessoal de Nível Superior – CAPES and the research grant given to the authors by the Conselho Nacional de Desenvolvimento Científico e Tecnológico – CNPq.

REFERENCES

[1] Sha W, Guo Z. Maraging steels: modelling of microstructure properties and applications. Oxford [Etc.]: Woodhead Publishing Limited; 2009.
[2] El-Fawkhry MK, Eissa M, Fathy A, Mattar T. Development of maraging steel with retained austenite in martensite matrix. Mater Today Proc 2015;2:S711–4, http://dx.doi.org/10.1016/j.matpr.2015.07.381.
[3] Masoumi M, de Barros IF, Herculano LFG, Coelho HLF, de Abreu HFG. Effect of microstructure and crystallographic texture on the Charpy impact test for maraging 300 steel. Mater Charact 2016;120:203–9, http://dx.doi.org/10.1016/j.matchar.2016.09.003.
[4] Jha AK, Sreekumar K, Tharian T, Sinha PP. Process optimization for high fracture toughness of maraging steel rings formed by mandrel forging. J Manuf Process 2010;12:38–44, http://dx.doi.org/10.1016/j.jmapro.2010.01.007.
[5] Buckingham RC, Argyrakis C, Hardy MC, Birosca S. The effect of strain distribution on microstructural developments during forging in a newly developed nickel base superalloy. Mater Sci Eng A 2016;654:317–28, http://dx.doi.org/10.1016/j.msea.2015.12.042.
[6] Castro Güiza GM, de Oliveira CaS. Microstructural changes produced by hot forging in a C300 Maraging Steel. Mater Sci Eng A 2015;655:142–51, http://dx.doi.org/10.1016/j.msea.2015.12.084.
[7] Samolyk G, Pater Z. Application of the slip-line field method to the analysis of die cavity filling. J Mater Process Technol 2004;153–154:729–35, http://dx.doi.org/10.1016/j.matprotec.2004.04.092.
[8] Schnitzer R, Radis R, Nöhrer M, Schober M, Hochfellner R, Zinner S, et al. Reverted austenite in PH 13-8 Mo maraging steels. Mater Chem Phys 2010;122:138–45, http://dx.doi.org/10.1016/j.matchemphys.2010.02.058.
[9] Hou H, Qi L, Zhao YH. Effect of austenitizing temperature on the mechanical properties of high-strength maraging steel. Mater Sci Eng A 2013;587:209–12, http://dx.doi.org/10.1016/j.msea.2013.08.070.
[10] Li K, Shan J, Wang C, Tian Z. Influence of aging temperature on strength and toughness of laser-welded T-250 maraging steel joint. Mater Sci Eng A 2016;669:58–65, http://dx.doi.org/10.1016/j.msea.2016.05.043.
[11] Abreu HFG, Tavares SSM, Silva JJM, Menezes JWA, Bruno AD. The influence of an intermediate austenitization heat treatment in the texture of cold-rolled and aged 18% Ni maraging steel. Mater Charact 2004;52:203–7, http://dx.doi.org/10.1016/j.matchar.2004.05.007.
[12] Mandal S, Tewary NK, Ghosh SK, Chakrabarti D, Chatterjee S. Thermo-mechanically controlled processed ultrahigh strength steel: microstructure, texture and mechanical properties. Mater Sci Eng A 2016;663:126–40, http://dx.doi.org/10.1016/j.msea.2016.03.127.
[13] Mitrofanov YP, Peterlechner M, Divinski SV, Wilde G. Impact of plastic deformation and shear band formation on the boson heat capacity peak of a bulk metallic glass. Phys Rev Lett 2014;112:1–5, http://dx.doi.org/10.1103/PhysRevLett.112.135901.
[14] Lima Filho VX, Barros IF, Abreu de HFG. Influence of solution annealing on microstructure and mechanical properties of maraging 300 steel. Mater Res 2017;20:10–4, http://dx.doi.org/10.1590/1980-5373-MR-2016-0257.
[15] Maistro G, Oikonomou C, Rogström L, Nyborg L, Cao Y. Understanding the microstructure-properties relationship of low-temperature carburized austenitic stainless steels through EBSD analysis. Surf Coat Technol 2017;322:141–51, http://dx.doi.org/10.1016/j.surfcoat.2017.05.036.
[16] Song R, Ponge D, Raabe D, Speer JG, Matlock DK. Overview of processing, microstructure and mechanical properties of ultrafine grained bcc steels. Mater Sci Eng 2006;441:1–17, http://dx.doi.org/10.1016/j.msea.2006.08.095.
[17] Umemoto M. Nanocrystallization of steels by severe plastic deformation. Mater Trans 2003;44:1900–11.
[18] Petch NJ. The cleavage strength of polycrystals. J Iron Steel Inst 1953;174:25–8, http://dx.doi.org/10.1007/BF01972547.
[19] Hall EO. The deformation and ageing of mild steel: III. Discussion of results. Proc Phys Soc Sect B 1951;64:747–53, http://dx.doi.org/10.1088/0370-1301/64/9/303.
[20] Mingard KP, Roebuck B, Bennett EG, Gee MG, Nordenstrom H, Sweetman G, et al. Comparison of EBSD and conventional methods of grain size measurement of hardmetals. Int J Refract Met Hard Mater 2009;27:213–23, http://dx.doi.org/10.1016/j.ijrmhm.2008.06.009.
[21] Lobanov ML, Danilov SV, Pastukhov VI, Averin SA, Khrunyk YY, Popov AA. The crystallographic relationship of molybdenum textures after hot rolling and recrystallization. Mater Des 2016;109:251–5, http://dx.doi.org/10.1016/j.matdes.2016.06.103.
[22] Semiatin SL, Weaver DS, Kramb RC, Fagin PN, Glavicic MG, Goetz RL, et al. Deformation and recrystallization behavior during hot working of a coarse-grain, nickel-base superalloy ingot material. Metall Mater Trans A 2004;35:679–93, http://dx.doi.org/10.1007/s11661-004-0379-y.
[23] Rollett A, Humphreys F, Rohrer GS, Hatherly M. Recrystallization and related annealing phenomena. 2nd ed; 2004, http://dx.doi.org/10.1016/B978-0-08-044164-1.X5000-2.
[24] Sainath G, Choudhary BK. Orientation dependent deformation behaviour of BCC iron nanowires. Comput Mater Sci 2016;111:406–15, http://dx.doi.org/10.1016/j.commatsci.2015.09.055.
[25] Blondé R, Jimenez-melero E, Huizenga R, Zhao L, Wright J, Bru E, et al. High-resolution X-ray diffraction investigation on the evolution of the substructure of individual austenite grains in TRIP steels during tensile deformation research papers. Mater Sci Eng A 2014;47:965–73, http://dx.doi.org/10.1107/S1600576714008553.
[26] Hielscher R, Mainprice D, Schaeben H. Material behavior: texture and anisotropy. In: Handb geomathematics. 2nd ed; 2015. p. 2149–88, http://dx.doi.org/10.1007/978-3-642-54551-1_33.
[27] Grilli N, Janssens KGF, Nellessen J, Sandlöbes S, Raabe D. Multiple slip dislocation patterning in a dislocation-based crystal plasticity finite element method. Int J Plast 2018;100:104–21, http://dx.doi.org/10.1016/j.ijplas.2017.09.015.
[28] Liang XZ, Dodge MF, Kabra S, Kelleher JF, Lee TL, Dong HB. Effect of hydrogen charging on dislocation multiplication in pre-strained super duplex stainless steel. Scr Mater 2018;143:20–4, http://dx.doi.org/10.1016/j.scriptamat.2017.09.001.
[29] Raabe D. Simulation of rolling texture of b.c.c. metals considering grain interaction and crystaloraphic slip on {100}, {112} and {123} planes. Mater Sci Eng A 1995;197:31–7, http://dx.doi.org/10.1016/0921-5093(94)09770-4.